Three Dimensional Finite Element Modeling of the Earth's Magnetosphere

Petr Kloucek and Frank R. Toffoletto

CRPC-TR98757
May 1998

Center for Research on Parallel Computation
Rice University
6100 South Main Street
CRPC - MS 41
Houston, TX 77005

Submitted August 1998; Also available as Rice CAAM TR 98-11

Three Dimensional Finite Element Modeling of the Earth's Magnetosphere

Petr Klouček *
Department of Computational and Applied Mathematics,
Rice University,
6100 Main Street, Houston, TX 77005, USA
E-mail: kloucek@rice.edu

and

Frank R. Toffoletto†
Department of Space Physics and Astronomy,
Rice University,
6100 Main Street, Houston, TX 77005, USA
E-mail: toffo@rice.edu

*This author was partially supported by the National Science Foundation, through the Center for Research on Parallel Computation, under Cooperative Agreement No. CCR-9120008, and by a grant from the NASA Goddard Space Flight Center.

†This author was partially supported by the National Science Foundation (GEM) grant ATM-9501898 and NASA grant NAG5-4726.

Abstract

We demonstrate the feasibility of using a nonconforming finite element method on an unstructured grid in solving a magnetospheric physics problem. We use this approach to construct a global discrete model of the magnetic field of the magnetosphere that includes the effects of shielding currents at the outer boundary (the magnetopause). As in the approach of [17] the internal magnetospheric field model is that of Hilmer and Voigt [3] while the magnetopause shape is based on an empirically-determined approximation [12]. The result is a magnetic field model whose field lines are completely confined within the magnetosphere. The numerical results indicate that the nonconforming discrete model is robust and efficient.

Keywords Magnetopause, magnetosphere, Chapman-Ferraro Currents, Nonconforming finite elements, Laplace's equation, Neumann boundary value problem

1991 Mathematical Subject Classification 65M60, 65N50, 65J10, 85A20, 85-08

1 Introduction

The Earth's magnetosphere is formed by the interaction of the solar wind with the Earth's magnetic field. This interaction, to zeroth-order, causes the solar wind to flow around the cavity carved out by the Earth's magnetic field forming the region known as the magnetosphere. The magnetospheric shape is compressed on the upstream or sunward side and stretched out to form a long tail in the downstream region. This solar-wind magnetosphere interaction produces currents both within the magnetosphere and at the boundary (the magnetopause). The magnetopause currents, often

called the Chapman-Ferraro Currents [2], confine the magnetospheric magnetic field lines within the magnetosphere in the idealized case of a closed magnetosphere considered here.

Let Ω be a three dimensional domain representing the Earth's magnetosphere, $\partial\Omega$ the magnetopause, and $\partial\Omega_{\mathrm{TAIL}}$ be the downstream boundary. We define the internal source magnetic field B_S for any $x \in \Omega$ to include (1) the magnetic field of Earth's dipole moment, (2) the tail field generated by currents flowing in the Earth's tail, (3) the ring current field which is generated by a region of trapped plasma in the near-Earth region. Note that the methods outlined here are general enough to be applicable to any magnetic field model. The Chapman-Ferraro field B_{CF} results from the shielding Chapman-Ferraro current at the magnetopause $\partial\Omega$. The total normal component at the magnetopause for a closed magnetosphere is then

$$(B_S(x) + B_{CF}(x)) \cdot n = 0, \qquad x \in \partial\Omega, \tag{1.1}$$

where n is the outward unit vector normal to the magnetopause $\partial\Omega$. The details of the Hilmer-Voigt magnetic field model B_S can be found in [3]. By definition, the Chapman-Ferraro field B_{CF} is curl-free in Ω, thus it can be computed as the negative gradient of a scalar potential Φ

$$B_{CF}(x) \stackrel{\mathrm{def}}{=} -\nabla\Phi(x), \qquad x \in \Omega. \tag{1.2}$$

Since the magnetic field B_{CF} is required to be divergence-free, we have

$$\Delta\,\Phi = 0, \qquad x \in \Omega. \tag{1.3}$$

The solution of the equation (1.3) subject to the boundary condition (1.1) is called the Chapman-Ferraro problem [2]. A general discussion of this problem and a review of early work can be found in [21] or [11].

A perturbation of this shielding process occurs when there is a small but finite normal component of the magnetic field at the magnetopause [15, 16]. The method we present here is applicable to an arbitrary magnetopause boundary condition and is readily adapted to the open magnetosphere modeling approach introduced in [15]. The open magnetosphere is modeled by replacing (1.1) with a non-homogeneous Neumann boundary condition.

If the magnetopause coincides with one of the coordinate surfaces (e. g. sphere) of a system in which Laplace's equation is separable [9], then Φ may be expanded in harmonic functions of that system and the coefficients may be derived by an inversion integral. Examples include spherical coordinates with a spherical magnetopause [22], parabolic coordinates with a paraboloid-of-revolution magnetopause [1, 13]; [18], and a combination of spherical and cylindrical coordinates with a hemispherical dayside magnetopause joined to a semi-infinite cylinder tail magnetopause [20, 22]. While these approaches have provided elegant and useful magnetic field models, the restrictions imposed by the technique limit the class of magnetopause shapes that can be considered. For example, the magnetopause shape that results from a magnetophydrodynamic pressure-balance calculation, where the shocked solar-wind pressure is balanced against the internal magnetic-field pressure, does not generally coincide with any of the shapes for which a separable solution to (1.3) can be found.

An alternative approach for non-separable solutions of (1.3) has been implemented in [14]. The coefficients are fitted to the boundary condition by least squares [14, 19]. A finite difference method has been used in [17] using a curvilinear grid but the technique is restricted to axis-symmetric magnetopause shapes.

2 The Finite Element formulation of the Chapman-Ferraro problem

Finite element approximation of the potential Φ of the Chapman-Ferraro magnetic field B_{CF} is based on the generalization of the spatially averaged non-conforming finite element introduced in [10]. This approximation has been extensively used in [4] to approximate almost everywhere discontinuous deformations associated with the Martensitic transformation. The numerical analysis of this finite

element has been done in [6]. This finite element does not have a conforming core making it special among a class of nonconforming finite elements.

2.1 The weak formulation of the Chapman-Ferraro problem

Let Ω be a bounded domain with Lipschitz boundary and let us assume that the necessary compatibility condition for the interior Neumann problem is satisfied, i.e.

$$\int_{\partial\Omega} B_S \cdot n \, dS = 0. \tag{2.1}$$

The boundary condition (1.1) yields the following weak formulation. The function $\Phi \in W^{1,2}(\Omega)$ is called the weak solution of the Chapman-Ferraro problem (1.3) with the homogeneous Neumann boundary condition (1.1) if

$$\int_{\Omega} \nabla\Phi(x)\nabla v(x)\, dx = \int_{\partial\Omega} B_S \cdot n \, v \, dS, \qquad \text{for any } v \in W^{1,2}(\Omega). \tag{2.2}$$

It is well-known that the interior Neumann problem (2.2) has at most one solution $\Phi \in C^2(\Omega) \cap C^1(\overline{\Omega})$ if $\partial\Omega \in C^1$. The solution is determined up to an arbitrary additive constant. The solution can be singled out by assuming any of the conditions $\int_\Omega u(x)\, dx = 0$ or $\int_{\partial\Omega} u \, dS = 0$ or by fixing the solution Φ at some point on $\partial\Omega$. For Ω with a polygonal boundary the solution of (2.2) is less smooth. In particular, the solution Φ is in $W^{2,2}(\Omega)$ if the angles among the boundary segments are strictly less than 180^o.

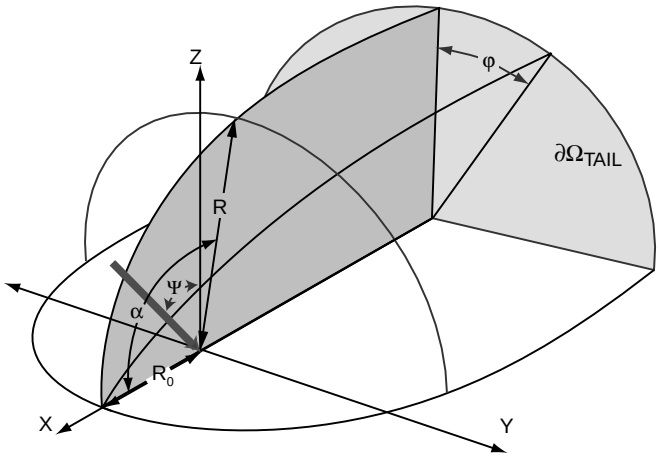

Figure 1: This Figure illustrates the geometry and the coordinate system used in this work where x points towards the sun. The angle φ is the cylindrical coordinate out of the $x-z$ plane. In this coordinate system, the Earth's dipole field tilts in the $x-z$ plane at an angle Ψ. The tail boundary is labeled $\partial\Omega_{\text{TAIL}}$

2.2 Magnetopause shape approximation

We have taken the Earth's magnetosphere Ω to have the boundary given by the function used in [12]. We approximate the magnetopause $\partial\Omega$ by the function

$$R_{mp}(x) = R_0 \left(\frac{2}{1 + cos(\alpha)} \right)^{\beta} \tag{2.3}$$

where (R_0) is a standoff distance, and α is an angle such that $\alpha = 0$ corresponds to the location $(x, y, z) = (R_0, 0, 0)$, cf. Fig.1. The parameter β determines the downstream flaring angle of the magnetopause, for simplicity a value of $\beta = 0.5$ is used.

The three-dimensional magnetospheric cavity is generated by a rotation about the x-axis to produce an axisymmetric magnetopause. Non-axisymmetric magnetopause shapes are modeled by making the magnetotail radius $R_{mp}(x)$ a function of the angle φ. For the Earth's magnetosphere, R_0 varies between $8-12$ Earth Radii (R_E) although during extreme solar wind conditions it can become as small as $4R_E$. For the cases presented here, a constant value of $10R_E$ was used.

2.3 The nonconforming finite element formulation

We partition the Earth's magnetosphere Ω with the magnetopause $\partial\Omega$ into quadrilaterals $Q_h \in \tau_h$ such that

$$\begin{aligned}
&\Omega_h \stackrel{\text{def}}{=} \bigcup_{Q_h \in \tau_h} Q_h, \qquad \text{where} \\
&\overline{\Omega}_h \subseteq \overline{\Omega}, \quad \partial^2\Omega_h \in \partial\Omega, \quad \lim_{h\to 0} \text{meas}(\Omega - \Omega_h) = 0, \qquad \text{and} \\
&\lim_{h\to 0_+} \frac{h}{\rho} < \infty, \qquad \text{where} \\
&\rho \stackrel{\text{def}}{=} \min_{Q_h} \text{diam}\, Q_h, \quad h \stackrel{\text{def}}{=} \max_{Q_h} \text{diam}\, Q_h.
\end{aligned} \tag{2.4}$$

The *averaged harmonic* finite element is defined by the triple (Q, P_Q, Σ_Q), where $Q \equiv [a-r, a+r] \times [b-s, b+s] \times [c-t, c+t]$ is a rectangular parallelopiped with its center at (a, b, c), and the lengths of its edges $2r$, $2s$, $2t$, where $r, s, t > 0$,

$$\begin{aligned}
P_Q &= \text{Span}\left\{1,\ x,\ y,\ z,\ \left(\frac{x}{r}\right)^2 - \left(\frac{y}{s}\right)^2, \left(\frac{x}{r}\right)^2 - \left(\frac{z}{t}\right)^2\right\}, \\
\Sigma_Q &= \left\{\frac{1}{|F_i|}\int_{F_i} q\, dS \,|\, i = 1, \ldots, 6\right\}.
\end{aligned} \tag{2.5}$$

Here $F_i,\ i = 1, \ldots, 6$, are the faces of the rectangular parallelopiped Q, and where $|F|$ denotes the area of the face F. This finite element is well defined since Σ_Q is P_Q-unisolvent. This can be easily checked by considering the six polynomials $\psi_i = \psi_i(x, y, z),\ i = 1, \ldots, 6$, obtained by permuting the terms $(x-a)/r$, $(y-b)/s$ and $(z-c)/t$ in the polynomial

$$-\frac{1}{4}\left(\frac{x-a}{r}\right)^2 - \frac{1}{4}\left(\frac{y-b}{s}\right)^2 + \frac{1}{2}\left(\frac{z-c}{t}\right)^2 + d\frac{z-c}{2t} + \frac{1}{6},$$

with $d = \pm 1$. It is obvious that $\psi_i \in P_Q, i = 1, \ldots, 6$, and it is easily checked that with a suitable labeling of the indices,

$$\frac{1}{|F_i|}\int_{F_i} \psi_j\, dS = \delta_{ij}.$$

Thus, $\{\psi_i\}_{i=1}^6$ is the standard basis for the finite element (Q, P_Q, Σ_Q). Now, we define a vector-valued polynomial space

$$P \times P \times P \stackrel{\text{def}}{=} \{(w_1(x), w_2(x), w_3(x)) \,|\, w_i(x) \in P_Q \ \text{ for } i = 1, 2, 3\}. \tag{2.6}$$

The finite element space V_h used to approximate in some sense the Sobolev space $W^{1,2}(\Omega)$ used in (2.2) is defined by the triple $\{Q, P_Q, \Sigma_Q\}$. Namely,

$$\begin{aligned} V_h \equiv \{\, & v_h \in L^2(\Omega_h) \,:\, v_h\big|_{Q_h} \in P_{Q_h},\ \forall Q_h \in \tau_h; \\ & \int_F v_h\big|_{Q_h'}\, dS = \int_F v_h\big|_{Q_h''}\, dS,\ \text{for any face } F = \partial Q_h' \cap \partial Q_h'' \neq \emptyset,\ Q_h', Q_h'' \in \tau_h \,\}. \end{aligned} \tag{2.7}$$

The weak formulation (2.2) with the definition (2.7) of the space V_h reads

$$\int_{\Omega_h} \nabla_h \Phi_h(x) \nabla_h v_h(x)\, dx = \int_{\Omega_h} B_S \cdot n v_h\, dS. \tag{2.8}$$

The discrete gradient operator ∇_h used in the formulation (2.8) is defined on $\Phi_h(x) \in V_h$ to be the function defined on Ω_h by applying the classical gradient differential operator ∇ in the subdomains Q_h and by neglecting the contribution of the gradient operator ∇ when applied across the faces of Q_h where $\Phi_h(x)$ is possibly discontinuous. In other words, we have that

$$\nabla_h \Phi_h(x) = \nabla \Phi_h(x) \qquad \text{for } x \in Q_h\,. \tag{2.9}$$

The discrete gradient operator ∇_h ignores the effect of the discontinuities of the potential $\Phi_h \in V_h$ when computing the gradient, so

$$\int_{\Omega_h} \nabla_h \Phi_h(x) \nabla_h v_h(x)\, dx = \sum_h \int_{Q_h} \nabla \Phi_h(x) \nabla v_h(x)\, dx.$$

The finite element defined through (2.5) in (2.7) is called *nonconforming finite element space* with respect to the second order problem (2.2) because $V_h \nsubseteq W^{1,2}(\Omega)$ as is required by the weak formulation. It follows from the continuity condition imposed in the definition of the space V_h (2.7) that there exists on each face of Q_h at least one connected curve such that the function Φ_h is continuous along this curve.

The idea behind the implementation of the nonconforming approximation for the solution of the elliptic problems is adaptivity. Our calculations serve as a precursor for the solution of the MHD equations. It has been demonstrated in [4], [5] that the finite element (2.5) is very well suited for the computations of phenomena that can be described by a function that has almost everywhere discontinuous gradient. In other words, it allows for good approximation of sharp discontinuities.

The shocks associated with the solutions of MHD are sharp to a first order approximation. Most of the field is smooth however. The calulations described in this paper demonstrate that both non-smooth and smooth solutions can be obtained via nonconforming calculations thus reducing computational expense.

Theoretically, the order of approximation using nonconforming finite elements is $O(h)$ due to omission of the values of Φ_h along cross-interelement boundaries, c.f. (2.9). The computations presented in this paper produce somewhat higher than expected smoothness.

We define subparametric family of averaged harmonic elements $\{Q_h, P_{Q_h}, \Sigma_{Q_h}\}$ using the invertible equivalence map $F \in (P_1(Q_{\rm ref}))^3$, i.e.

$$\begin{aligned} &Q_h = F(Q), \\ &P_{Q_h} = \{p_h \,|\, p_h : Q_h \to \mathbb{R},\, p_h = q \circ F^{-1}, q \in P_Q,\, p \in P_{Q_h}\}, \qquad \text{and} \\ &\Sigma_{Q_h} = \{\frac{1}{|F_{h,i}|}\int_{F_{h,i}} p_h \, dS : i = 1, \ldots, 6\}. \end{aligned} \tag{2.10}$$

Working with Span$\{1, x, y, x^2 - y^2, x^2 - y^2\}$ would not yield properly defined finite element for anything other than the cube $[-r, r]^3$, $r > 0$. Therefore the choice of this polynomial space does not yield an affine family of finite elements. This difficulty is removed by scaling the spatial variables by r, s, t, c.f. the definition (2.5). The scaled averaged harmonic finite element is well defined for any rectangular parallelopiped forming an affine family under the equivalence mapping $F \in (P_1(Q_{\rm ref}))^3$. Unfortunately, this finite element does not form a subparametric family under the equivalence mapping $F \in (Q_1(Q_{\rm ref}))^3$. $F \in (P_1)^3$ even though the partition τ_h of Ω_h requires trilinear transformation on the referential rectangular parallelpiped. The analysis shows that further nonconformity thus created is confined within the realm of $O(h)$ error. The definition (2.5) of the averaged scaled harmonic finite element is "non-local" in a sense that the referential basis functions change with respect to the actual corresponding element Q_h.

We note that in general $\Delta\,\phi \neq 0$ for $\phi \in P_Q$ unless $r = s = t$. Therefore we have included a rectangular parallelopipeds Q_h inside the magnetosphere Ω_h to impose point-wise the divergence-free condition (1.3). The partition of Ω_h is visualized in Fig.2. Note that a finite element method

usually delivers only averaged values of computed quantities. The unexpected continuity mentioned above is related to the harmonicity imbedded into the definition (2.5).

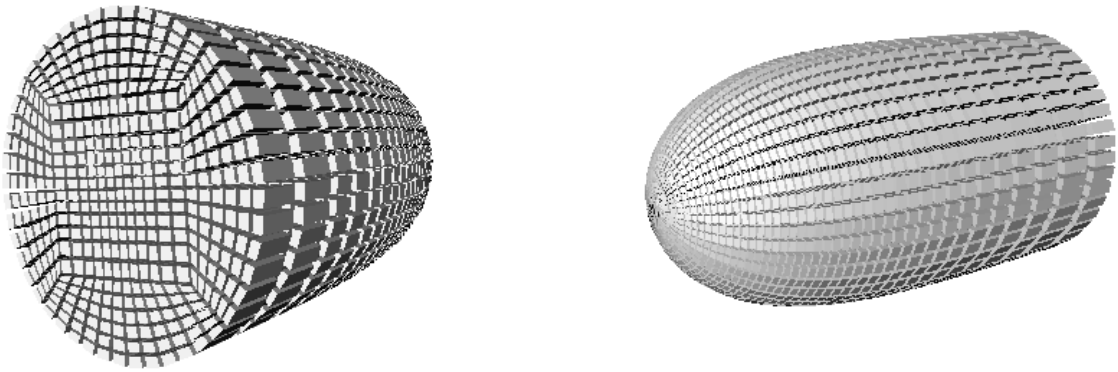

Figure 2: The computational magnetosphere Ω_h. The left figure highlights the tail of the domain that shows imbedded cubes Q_h where the finite element (2.5) is harmonic. In this figure, each particular element Q_h is shrunk by about 30% to illustrate that the partition τ_h is isoparametricaly equivalent to a single rectangular parallelopiped under a map $F \in (Q_1(Q_{\rm ref}))^3$, where Q_1 is the set of trilinear forms.

3 Calculations with zero tilt

Computation of the magnetic field with zero tilt ($\Phi = 0$), i.e. when the source magnetic field B_S points in the direction $(0, 0, -1)$ constitutes a mathematically and physically simpler problem. In this model the tail is truncated at some finite downstream distance (cf. Fig.1, $\partial\Omega_{\rm TAIL}$) where the simple boundary condition $B_{CF}(x) \cdot n = 0$ for all x on $\partial\Omega_{\rm TAIL}$ is used.

The calculations have been done with a low spatial resolution to provide sufficient computational evidence of the efficiency of the method. Namely, we take the $x-$direction resolution h_x to be $80/21$, and $h_y = h_z \sim 40/12$, measured at the diameter of Ω_h. The numerical integration associated with evaluation of the variational integrals in (2.8) is done using a Hammer and Stroud cubature formula that is accurate up to polynomials of order 5. This cubature rule requires 14 cubature points. The

partition τ_h in combination with the presented finite element and high-order numerical integration yields a system matrix A_h representing the system (2.8) with low condition number.

The discrete weakly harmonic solution to (2.8) must be symmetric. The fieldlines are computed using an Euler integration routine with adaptive stepsize. The result is shown in Fig.3 which represents the $x-z$ view of the computed fieldlines. One of the important tests of the solution Φ_h is to check if the fieldlines corresponding to $\nabla\Phi_h$ which originate in a plane stay in this plane. The nonconforming approximation allows for a lot of freedom in this sense. The fieldlines stay within a range of $y = \pm 0.05$ except for the fieldlines that pass extremely close to the singularity in B_s. This means that lateral approximation error is about 0.1% which is well beyond the $y-$direction resolution $h_y \sim 3\frac{1}{3}$. The lateral numerical stability seems to be a consequence of the point-wise harmonicity of the spatial approximation.

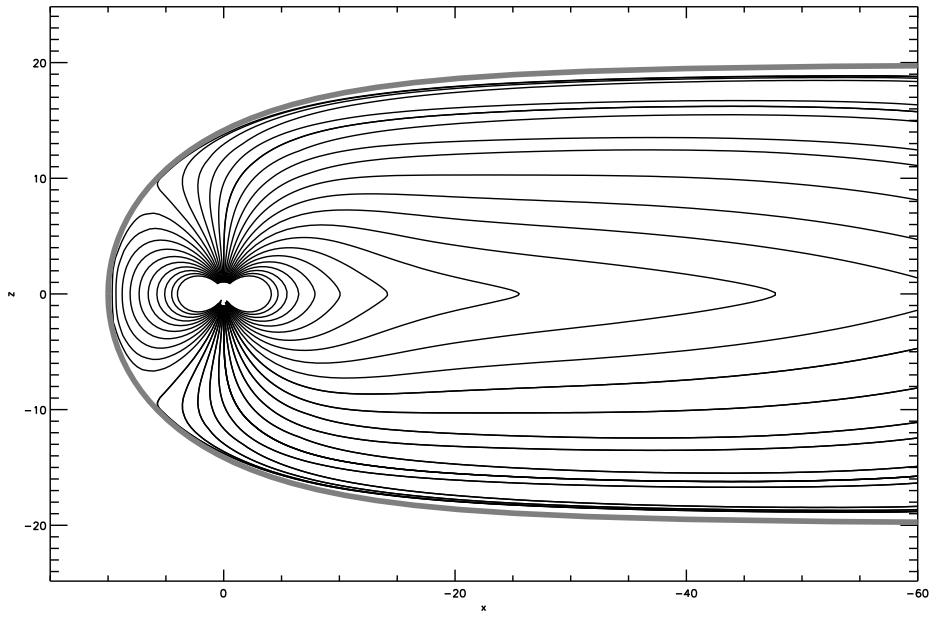

Figure 3: The fieldlines given by the computed solution $\nabla\Phi_h$ in the $x-z$ plane. The outer heavy line represents the magnetopause location.

4 Calculations with nonzero tilt

When the dipole tilt angle Φ is nonzero we have

$$\int_{\partial\Omega} B_S \cdot n \, dS \neq 0. \tag{4.1}$$

The non-zero boundary flux violates the basic necessary compatibility condition for the interior Neumann problem. The amount of the flux B_S through the tail region $\partial\Omega_{\rm TAIL}$ is not known a priori. We compensate this deficiency as follows. Let b be the total flux of B_S, i.e.,

$$\begin{aligned} b &\stackrel{\rm def}{=} \int_{\partial\Omega} B_S \cdot n \, dS = \int_{\partial\Omega\setminus\partial\Omega_{\rm TAIL}} B_S \cdot n \, dS + \int_{\partial\Omega_{\rm TAIL}} B_S \cdot n \, dS \\ &= \int_{\partial\Omega\setminus\partial\Omega_{\rm TAIL}} B_S \cdot n \, dS + B_S^{\rm TAIL} \, {\rm meas}(\partial\Omega_{\rm TAIL}). \end{aligned} \tag{4.2}$$

Here, $\partial\Omega_{\rm TAIL}$ refers to the cut-off of the computational domain with the outer normal $n = (1, 0, 0)$ and ${\rm meas}(\partial\Omega_{\rm TAIL})$ represents the area of this region. For an axisymmetric magnetopause we have ${\rm meas}(\partial\Omega_{\rm TAIL}) = \pi R_{\rm TAIL}^2$ for the simple computational region ploted on Fig.2. $R_{\rm TAIL}$ is the radius of the domain $\partial\Omega_{\rm TAIL}$. We want to find a value $\overline{B_S^{\rm TAIL}}$ such that

$$0 = \int_{\partial\Omega\setminus\partial\Omega_{\rm TAIL}} B_S \cdot n \, dS + \overline{B_S^{\rm TAIL}} \, {\rm meas}(\partial\Omega_{\rm TAIL}). \tag{4.3}$$

Let $(B_S^{\rm TAIL})_m$ be the $m-$th approximation of $\overline{B_S^{\rm TAIL}}$. We define the $(m+1)$st total flux b_{m+1} by

$$b_{m+1} \stackrel{\rm def}{=} \int_{\partial\Omega\setminus\partial\Omega_{\rm TAIL}} B_S \cdot n \, dS + (B_S^{\rm TAIL})_m \, {\rm meas}(\partial\Omega_{\rm TAIL}). \tag{4.4}$$

In view of (4.3) we approximate

$$-(B_S^{\rm TAIL})_{m+1} \, {\rm meas}(\partial\Omega_{\rm TAIL}) \sim \int_{\partial\Omega\setminus\partial\Omega_{\rm TAIL}} B_S \cdot n \, dS. \tag{4.5}$$

Hence, (4.4) and (4.5) yield the following fixed-point iteration scheme

$$(B_S^{\rm TAIL})_{m+1} = (B_S^{\rm TAIL})_m - b_{m+1} / \, {\rm meas}(\partial\Omega_{\rm TAIL}). \tag{4.6}$$

An example of a magnetic field configuration where the dipole field is tilted by 35° is shown in Fig.3. A three-dimensional perspective plot is shown in Fig.1. Note that for non-zero tilt the Hilmer-Voigt magnetic field model also displaces the tail field off the $x-y$-plane. In both figures the heavy lines denote the location of the magnetopause.

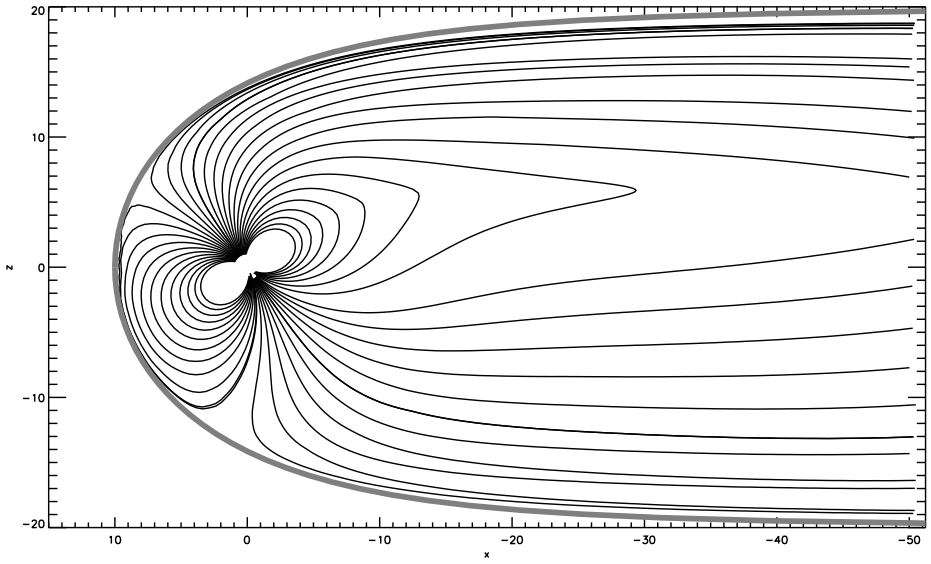

Figure 4: The fieldlines corresponding to the dipole field tilted by 35°.

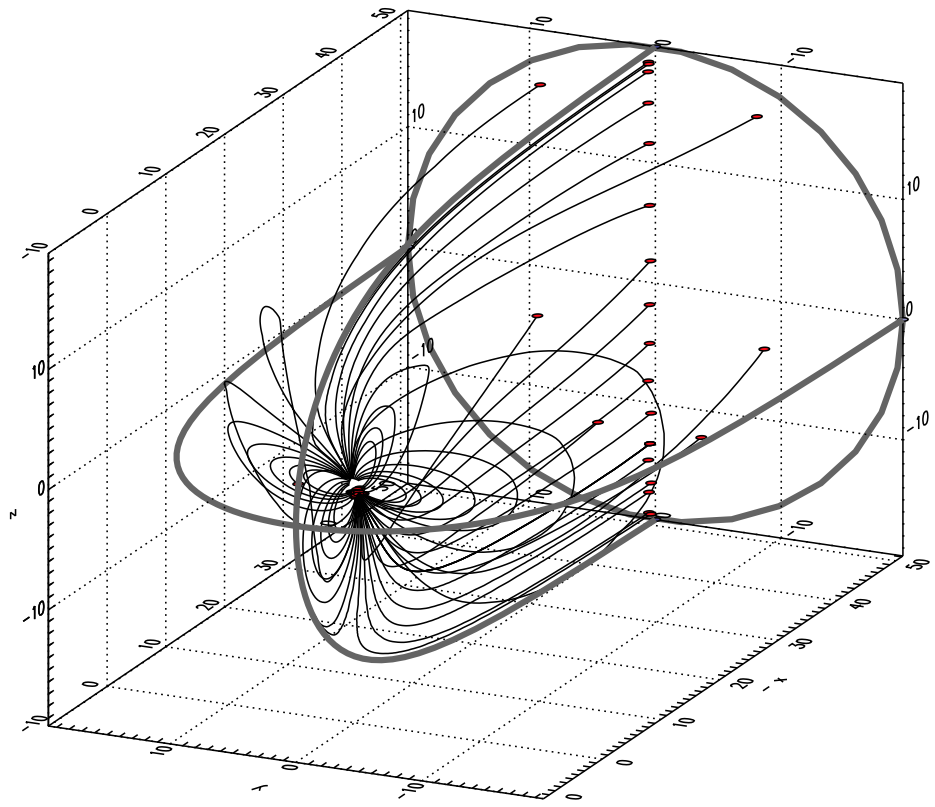

Figure 5: Three-dimensional plot of the final field configuration for the tilted dipole field. The heavy lines illustrate the location of the magnetopause.

5 Calculations with a non-axisymmetric magnetopause

A further application of our discrete model is the computation of a configuration where the magnetopause shape is no longer axisymmetric. In this case, the methods described in the previous section are the same with the exception that meas($\partial\Omega_{\text{TAIL}}$) becomes the cross-sectional area of $\partial\Omega_{\text{TAIL}}$. Pressure balance considerations indicate that the magnetopause should be indented in a region where the magnetic field is a minimum (the cusp); such an indentation has been modeled and is shown in Fig.6. The resulting field line configuration is shown in Figs.7,8. Figure 8 shows that the y-extent has been compressed.

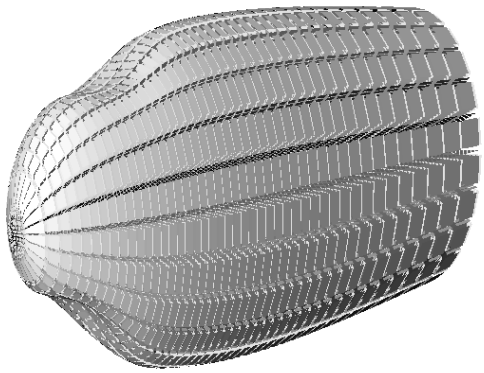

Figure 6: Grid configuration for the case of a non-axisymmetric magnetopause.

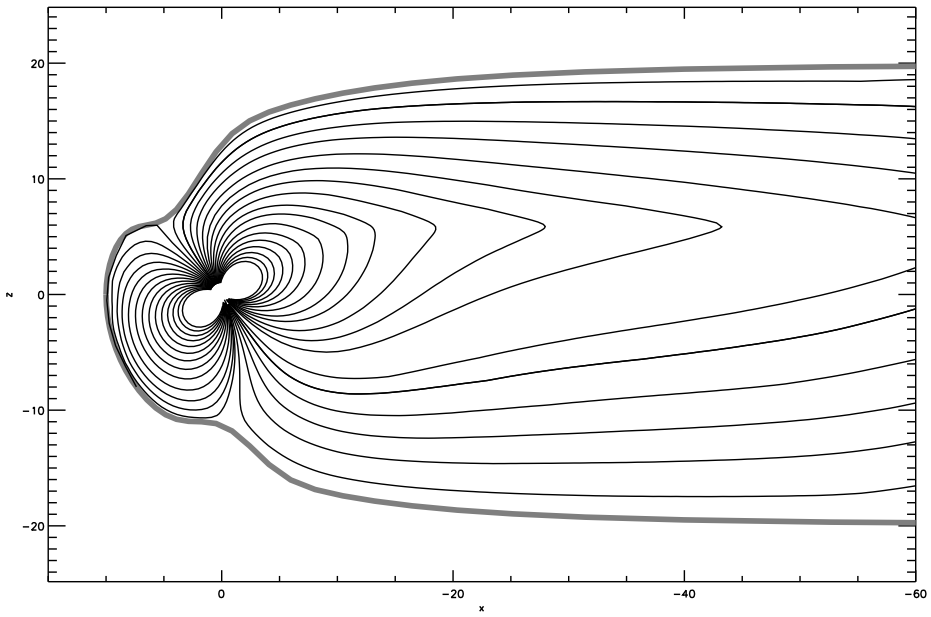

Figure 7: Fieldline plots as viwed in the $x-z$ plane for the case of a non-axisymmetric magnetopause; the indentations were placed near the local minimum in the magnetic field, the location of which is asymmetric with respect to z. The outer-heavy line represents the magnetopause location.

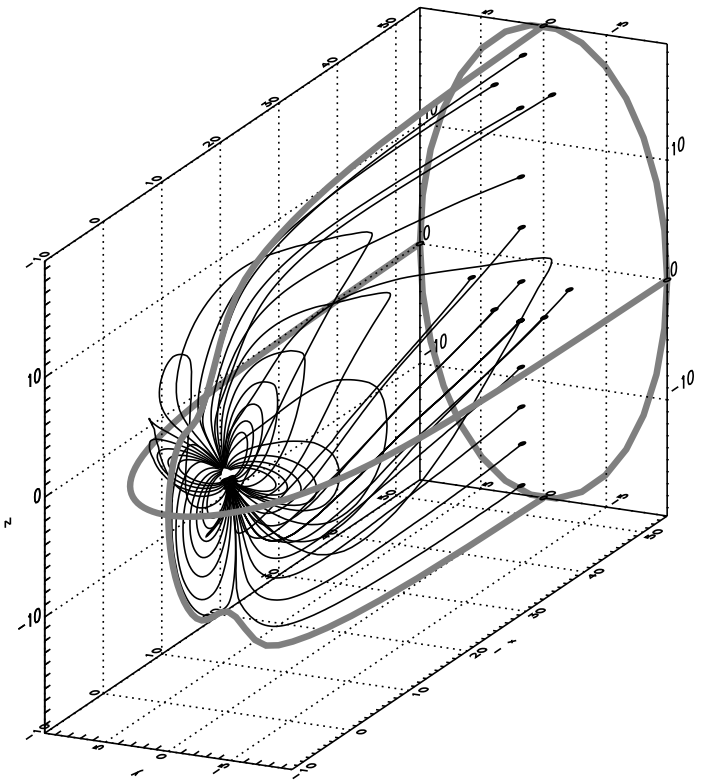

Figure 8: Fieldline plots as viewed in a three-dimensional perspective plot for the case of a non-axisymmetric magnetopause. The outer-heavy line represents the magnetopause location. The indentations are placed near minima in the internal magnetic field.

6 Summary and Conclusions

We have used a nonconforming finite-element method to generate a discrete magnetospheric field model. This type of technique is a generalization and extension of previous work and has potentially useful applications in magnetospheric modeling. The numerical calculations indicate that even nonconforming finite elements can be successfully used to approximate continuous quantities. The resulting method presented in this paper proves to be robust and to a large extent independent of the underlying unstructured grid. The local harmonicity of the finite elements used in our calculations proves to be useful in maintaining the symmetry of the solution even close to the singularity.

Our discrete method can be used to extend and generalize empirically-based magnetic field [19] and theoretical models [16] by allowing arbitrary magnetopause shapes to be used in calculations.

References

[1] Alekseev, I., I., and V. P. Shabansky, A model of a magnetic field in the geomagnetosphere, *Planet. Space Sci.*, 117-133 (20) (1972)

[2] Chapman, S., and V. C. A. Ferraro, A new theory of magnetic storms, Nature, 129-130 (126) (1930)

[3] Hilmer, R. V., and G. -H. Voigt, A magnetospheric magnetic field model with flexible current systems driven by independent physical parameters, *J. Geophys. Res.*, (1995)

[4] Klouček, P. and Luskin M., The computations of the dynamics of the Martensitic deformation *Continuum Mechanics and Thermodynamics* (6) (1994)

[5] Klouček, P., and Luskin M., Computational modeling of the Martensitic transformation with surface energy *Mathematical and Computer Modelling* (20(10/11)) (1994)

[6] Klouček,P, Li. B, and Luskin M., Nonconforming finite element approximation of the microstructure, *Math. Comp.* (65) 215 (1996)

[7] Koitchev, D. K. M. S. Kaschiev, Kartelev, M. D. Finite Element Numerical Modeling of Stationary Two-dimensional Magnetosphere with Defined Boundary, *J. Comput. Phys.*, (119), 220, (1995).

[8] Kartelev, M. D. M. S. Kaschiev, and D. K. Koitchev, Simplified 3D Magnetospheric Field, submitted to *J. Comput. Phys.*, (1998).

[9] Moon, P., and D. E. Spencer, *Field Theory Handbook*, Springer-Verlag, (1988)

[10] Rannacher, R. Turek S. Simple nonconforming quadrilateral Stokes element, *Numer. Meth. for PDEs* (8) (1992)

[11] Siscoe, G. L., The magnetospheric boundary. *In Physics of Space Plasmas (1987)* T. Chang, G. B. Crew, and J. R. Jasperse (Eds.), 3-78, Cambridge, Mass., Scientific Publishers, Inc. (1988).

[12] Shue, J. J. K. Chao, H. C. Fu. C. T. Russell, P. Song. K. K. Khurana, and HJ̇. Singer, A new functional form to study the solar wind control of the magnetopause size and shape. *J. Geophys. Res.*, (102), A5, 9497-9511, (1997).

[13] Stern, D. P. Parabolic harmonics in magnetospheric modeling: The main dipole and the ring current. *J. Geophys. Res.* 10851-10863 (90) 13, (1985).

[14] Schulz, M., and M. C. McNab, Source-surface model of the magnetosphere, *Geophys. Res. Lett.*, 182-185, (14) (1987)

[15] Toffoletto, F. R., and T. W. Hill, Mapping of the solar wind electric field to the Earth's polar caps, *J. Geophys. Res.*, (94) 329-347 (1989)

[16] Toffoletto, F. R., and T. W. Hill, A non-singular model of the open magnetosphere, *J. Geophys. Res.*, 1339-1344, (98) (1993)

[17] Toffoletto, F. R. Hilmer, R. V. Hill, T. W. and Voigt, G.H. Solution of the Chapman-Ferraro problem with an arbitrary magnetopause. *Geophys. ResLett.*, (21), 7, 621, (1994)

[18] Tsyganenko, N. A., A solution of the Chapman-Ferraro problem for an ellipsoidal magnetopause, *Planet. Space Sci.*, (37), 1037-1046, (1989)

[19] Tsyganenko, NÀ. Modeling the Earth's magnetospheric magnetic field confined within a realistic magnetopause. *J. Geophys. Res.*, (100), A4, 5599-5612, (1995).

[20] Voigt, G. -H., A three dimensional, analytical magnetospheric model with defined magnetopause, *Z. Geophys.*, (38), (1972)

[21] Voigt, G.H., Magnetospheric equilibrium configurations and slow adiabatic convection, in *Solar Wind-Magnetosphere Coupling*, edited by Y. Kamide and J. A. Slavin, p. 233, Terra Scientific, Tokyo, (1986).

[22] Voigt, G. -H., A mathematical magnetospheric field model with independent physical parameters, *Planet. Space Sci.*,1, (29) (1981).